

Structural studies of high dispersion H₃PW₁₂O₄₀/SiO₂ solid acid catalysts†

Andrew D. Newman,^a D. Robert Brown,^b Prem Siril,^b Adam F. Lee^a and Karen Wilson^{*a}

Received 17th March 2006, Accepted 22nd May 2006

First published as an Advance Article on the web 30th May 2006

DOI: 10.1039/b603979k

Highly dispersed H₃PW₁₂O₄₀/SiO₂ catalysts with loadings between 3.6 and 62.5 wt% have been synthesised and characterised. The formation of a chemically distinct interfacial HPW species is identified by XPS, attributed to perturbation of W atoms within the Keggin cage in direct contact with the SiO₂ surface. EXAFS confirms the Keggin unit remains intact for all loadings, while NH₃ adsorption calorimetry reveals the acid strength >0.14 monolayers of HPW is loading invariant with initial $\Delta H_{\text{ads}} = \sim -164 \text{ kJ mol}^{-1}$. Lower loading catalysts exhibit weaker acidity which is attributed to an inability of highly dispersed clusters to form crystalline water. For reactions involving non-polar hydrocarbons the interfacial species where the accessible tungstate is highest confer the greatest reactivity, while polar chemistry is favoured by higher loadings which can take advantage of the H₃PW₁₂O₄₀ pseudo-liquid phase available within supported multilayers.

Introduction

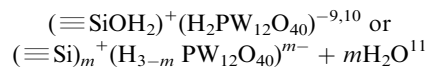
Numerous industrial chemical syntheses proceed through the stoichiometric application of homogeneous acids, bases or salts. Such methodologies generate large volumes of contaminated and often hazardous waste, with accompanying treatment and disposal costs.¹ Coupled with tightening legislation on the industrial management of such toxic waste, there is a strong drive towards alternative cleaner technologies for many liquid phase fine and speciality chemical processes. Heterogeneous catalysis offers particular promising solutions to these problems. A number of solid or supported materials are known with high acid/base strengths comparable to their currently employed homogeneous counterparts, and applicable as green replacements for undesirable homogeneous acids (*e.g.* H₂SO₄, AlCl₃, ZnCl₂ and BF₃).

Among heterogeneous acid catalysts under investigation, the group of materials known as heteropoly acids (HPAs) are particularly promising since they possess high Brønsted acid strengths (approaching the superacidic region) as well as tuneable redox activity depending on the particular constituent elements. Heteropoly acids are polyoxometalate inorganic cage structures, which may adopt the Keggin form with the general formula H₃MX₁₂O₄₀, where M is the central atom and X the heteroatom. Typically M can be either P or Si, and X = W or Mo. The highest stability and strongest acidity is

observed for phosphotungstic acid (H₃PW₁₂O₄₀). Several review articles on the general properties and chemistry of these materials are available.^{2–4}

While the acid properties of heteropoly acids have excited much interest, their inherent low surface area (1–5 m² g⁻¹) often necessitates support on a porous carrier.² Neutral or acidic supports are desirable since basic materials such as alumina can decompose the HPA structure and lower the catalyst acidity.² Various supports have been trialled, including molecular sieves,^{4,5} zeolites,⁶ zirconia⁷ and activated carbons,^{4,8} however silica is most often used since it is widely available, neutral or mildly acidic, and possesses specific (tuneable) surface areas and porosity.

Despite the importance of developing high area, dispersed HPA catalysts, almost nothing is known about the growth mode or physico-chemical properties of polyoxometalates over silica supports. It has been hypothesised that in the initial stages of impregnation, the HPA material reacts with a hydroxylated silica surface to form an ion pair with one or more silanol *via* simple proton transfer, possibly involving dehydration:



however attempts to discern these surface HPA species using ³¹P-MAS NMR (a non-surface sensitive technique) have proven inconclusive.^{2,4,9}

This work reports on the evolution of H₃PW₁₂O₄₀ (HPW) adlayers over a porous, hydroxylated silica using both bulk and surface sensitive techniques. The activity of these catalysts in reactions with non-polar and polar hydrocarbons such as liquid phase rearrangement of α -pinene and vapour phase condensation of methanol are used to probe the role of surface and bulk HPW species in catalysis.

^a Department of Chemistry, University of York, Heslington, York, UK YO10 5DD. E-mail: kw13@york.ac.uk; Fax: +44 1904 432516; Tel: +44 1904 432586

^b Department of Chemical & Biological Sciences, University of Huddersfield, Queensgate, Huddersfield, UK HD1 3HD. Fax: +44 1484 472182; Tel: +44 1484 473397

† Electronic supplementary information (ESI) available: Raw EXAFS spectra for HPW and reference compounds. See DOI: 10.1039/b603979k.

Experimental

Catalyst preparation

A series of silica-supported phosphotungstic acid catalysts were prepared with HPW loadings over the range 3.6–63 wt%. Simple wet impregnation was employed, involving dissolution of the required amount (0.25–9 g) of $\text{H}_3\text{PW}_{12}\text{O}_{40}$ (Aldrich, W content 70.1 wt%) in 50 cm³ methanol in a round-bottomed flask, followed by addition of (Fisher 100 Å) silica powder support material (2.5–10 g). The resulting mixture was left overnight followed by evaporation to a dry, free flowing powder at ~60 °C under vacuum. No further pre-treatments were applied to any catalysts, which were stored in air prior to analysis and reaction testing unless otherwise stated.

Catalyst characterisation

Elemental analysis was undertaken on a Fisons ICP-OES instrument, with water content (both physisorbed and crystalline) calculated by thermogravimetric analysis (TGA) using a Stanton Redcroft STA-780 between 20–700 °C. Nitrogen porosimetry measurements were performed on a Micromeritics ASAP 2010 instrument. Surface areas were calculated using the BET equation over the range $P/P_0 = 0.02$ – 0.2 , where a linear relationship was maintained, while pore size distributions were calculated using the BJH model up to $P/P_0 = 0.6$. Approximate calculation of the monolayer coverage is based on the average area per anion for (100) planes of 2D arrays on HOPG, and that of the bulk $\text{H}_3\text{PW}_{12}\text{O}_{40}$ structure of 144 Å².¹²

Diffuse reflectance IR (DRIFT) spectra were obtained using a Bruker Equinox 55 FTIR spectrometer equipped with an environmental cell. Pyridine titrations were carried out by addition of 2 cm³ neat pyridine to 100 mg of each catalyst, followed by drying at room temperature. Samples were diluted with KBr powder (2 wt%), then loaded into the cell and subjected to a vacuum at 70 °C prior to measurement. Samples were analysed utilising the Kubelka–Munk approximation to derive peak areas for reproducible quantitative analysis.

Hammett acidity¹³ measurements were undertaken by adding 5 cm³ indicator solution in cyclohexane to a weighed sample of HPA on silica so that each test sample contained 100 mg silica (total weight varied depending on HPW loading). Simple colour changes were noted visibly and after filtration using diffuse reflectance UV (DRUV) spectra which were undertaken on the dry, indicator absorbed catalyst using a Jasco V-550 UV spectrophotometer. The following Hammett indicators were used: phenylazoaniline ($H_0 = +2.8$), dicinnamalacetone ($H_0 = -3.0$), benzalacetophenone ($H_0 = -5.6$), anthraquinone ($H_0 = -8.2$), 4-nitrotoluene ($H_0 = -11.35$) and 2,4-dinitrotoluene ($H_0 = -13.75$). The acid strength is quoted as being stronger than the weakest indicator which exhibits a colour change, but weaker than the strongest base that produces no change.

X-Ray photoelectron spectroscopy (XPS) was performed on a Kratos AXIS HSi instrument equipped with a Mg K α anode and charge neutraliser. An analyser pass energy of 20 eV and X-ray power of 160 W were employed. Two point energy referencing was performed using adventitious carbon and the

valence band. Elemental compositions were determined using the appropriate response factors.

X-Ray diffraction was performed using a Philips 1800 Diffractometer (PH 03) with Cu K α radiation. Spectra were recorded in reflection mode from 20–80° at a scanning rate of 2° per minute with a step size of 0.04°.

X-Ray absorption spectra (XAS) were recorded on Station 9.3 at Daresbury, utilising synchrotron radiation of 2 GeV and > 125 mA current. W L_{III} data were recorded in transmission mode employing a Si(220) monochromator set at 70% harmonic rejection, typically over 20 min. Spectra were baseline subtracted and fitted using Daresbury EXSPLINE and Excurv98 packages, employing Fourier filtering over the range 0–12 Å. Samples were prepared in 2 mm stainless washers sealed with Sellotape and, where necessary, diluted with boron nitride to maintain the total absorbance around unity.

Flow adsorption calorimetric studies were made in a flow-through differential scanning calorimeter (Setaram DSC111) connected to gas flow and switching systems. Gas flow rates are controlled by automated mass flow controllers. The sample (5–60 mg) is held on a glass frit in a vertical silica glass sample tube in the calorimeter. A steady 5 ml min⁻¹ flow of He is maintained across the sample for 4 h at 150 °C to effect activation. A sequence of pulses of probe gas (1% NH₃ in He) is then delivered to the carrier gas stream from a 0.5 ml sample loop using a two position Valco[®] valve with an automated micro-electric actuator. Heat output associated with interaction between NH₃ and sample is detected with the DSC and the concentration of NH₃ in the gas flow downstream of the DSC is measured with a Hiden mass spectrometer gas analyser (HPR 20) connected through a heated capillary at 175 °C. A pulse delay (~30 min) is employed to allow reversibly adsorbed NH₃ to desorb back into the pure He stream and/or redistribute on the sample, and for the baselines to stabilise. The net amount of ammonia irreversibly adsorbed from each pulse can be determined by comparing the MS signal during each pulse with a signal recorded during a control experiment through a blank sample tube at the same temperature.

Reactivity

α -Pinene isomerisation was performed in a Radley's carousel reaction station under air at 30 °C. 100 mg of catalyst was added to 63 mmol of α -pinene (98%, Aldrich), with 0.1 cm³ of tetradecane (99%, Lancaster) added as an internal standard. Stirred reactions were run for 8 h with samples taken at regular intervals for analysis by a Varian CP-3800 gas chromatograph with CP-8400 autosampler using a DB1 capillary column (30 m \times 0.53 μ m). The principal major products were camphene and limonene, along with traces of terpinene, *para*-cymene and terpinolene in accordance with the literature.^{14,15} Catalyst selectivity and overall mass balances (closure > 98%) were determined using reactant and product response factors derived from multi-point calibration curves. The systematic errors in conversions and selectivities are ± 2 and $\pm 3\%$.

Gas phase reaction of MeOH to form DME was undertaken in a continuous plug-flow microreactor using a 1/2" glass tube packed with 0.25 cm³ catalyst. Helium was passed over the bed

at $40 \text{ cm}^3 \text{ min}^{-1}$ ($\text{GHSV } 9600 \text{ h}^{-1}$) during initial heating to $80 \text{ }^\circ\text{C}$, and MeOH was then added to the stream *via* a peristaltic pump at $1.2 \text{ cm}^3 \text{ h}^{-1}$ liquid ($19 \text{ mol}\%$ of gas flow). Following steady state baseline measurement, the temperature was ramped to $300 \text{ }^\circ\text{C}$ at $5 \text{ }^\circ\text{C min}^{-1}$, then held for 30 min to monitor deactivation. Reactions occurred at atmospheric pressure. Products were detected by online GC (Carboxen 1006 Plot column $30 \text{ m} \times 0.53 \text{ }\mu\text{m}$ film) and mass spectrometry, using a Shimadzu GC-14B and a VG 300 amu Mini-Torr quadrupole mass spectrometer, respectively. Both systems were PC interfaced for data acquisition. All lines were heated to $\sim 80 \text{ }^\circ\text{C}$ to ensure components remained gaseous for analysis. Temperatures for 50% conversion ($T_{50\%}$) were used to indicate the relative activity of the catalysts.

Results and discussion

Catalyst characterisation

Successful supporting of the HPW was first confirmed by elemental analysis on the catalyst series (Table 1). This revealed a progressive increase in W and P content with nominal HPW loading. The W : P molar ratio remained approximately constant across the series at $\sim 12 : 1$, in excellent agreement with that of the parent 12-phosphotungstic acid. The actual and nominal HPW loadings are corrected for the presence of crystalline water within the parent HPW structure, the formula of which was evaluated as $\text{H}_3\text{PW}_{12}\text{O}_{40} \cdot 6\text{H}_2\text{O}$ from TGA (see below) and represents the most stable and common crystalline form reported in the literature.

Fig. 1 shows the variation of surface W loading, from XPS, together with catalyst surface area, both as a function of bulk HPW content. As the overall loading of HPW increases the surface W coverage rose steadily, reaching a plateau of around 12 wt% surface W for bulk HPW loadings in excess of 43.5 wt%. A progressive decrease in catalyst surface area from 387 to $62 \text{ m}^2 \text{ g}^{-1}$ occurs across the series of supported HPW samples. However, due to the high density of the incorporated HPW surface areas of the final material are distorted at high loadings. To separate the effects of pore blockage from simple incorporation of a dense component, surface areas are normalised to the amount of SiO_2 present in each sample and reported in units of m^2 per gram of SiO_2 . This reveals that the surface area is initially decreasing upon HPW incorporation reaching a plateau over the range 20–43.5 wt%, prior to decreasing again for higher loadings. Porosimetry revealed the average pore diameter remained between 140–150 Å up to a

Table 1 Bulk composition of SiO_2 supported HPW catalysts

Nominal HPW loading wt%	Actual HPW loading wt%	Bulk P (ICP) wt%	Bulk W (ICP) wt%	W : P molar ratio
0	0	0	0	—
5	3.6		2.6	—
10	6.2	0.05	4.4	14.8
17	10.3	0.10	7.2	12.1
33	26.0	0.30	18.2	12.9
50	43.5	0.40	30.6	12.9
60	49.9	0.50	35.4	11.9
70	62.5	0.60	44.2	12.4

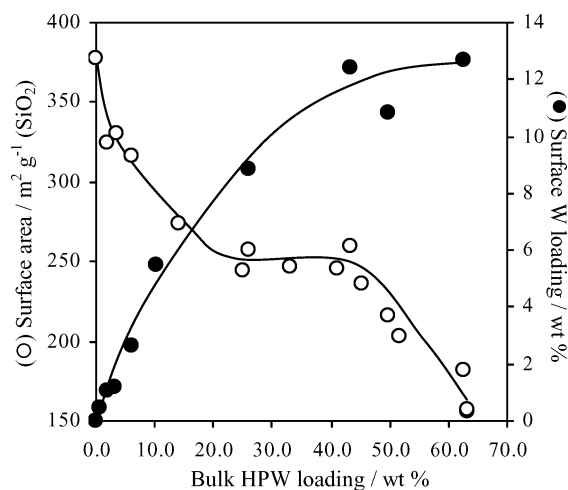


Fig. 1 Variation of surface W content and surface area of HPW/ SiO_2 as a function of HPW loading.

HPW loading of 43.5 wt%, suggesting the heteropoly acid phase remained well dispersed. The initial loss in surface area is thus attributed to the blocking of micropores. At higher loadings a decrease in pore diameter from 140 to 110 Å is observed coincident with the loss of surface area over this regime and is attributed to gradual blockage of the mesopore structure. Calculation of the surface area occupied by a close packed array of Keggin units of cross sectional area 14.4 nm^2 reveal that a loading of 43.5 wt% corresponds to a monolayer of HPW,¹⁶ suggesting the plateau in surface W content and point where the surface area decreases correspond to the point at which 3-dimensional heteropoly acid clusters begin to form. Additional HPW must encapsulate and screen the XP contribution from the initially deposited phase—indicative of multilayer or 3D crystallite growth.

TGA of unsupported and supported HPW species (Fig. 2), reveals that decomposition occurs in 3 distinct processes.

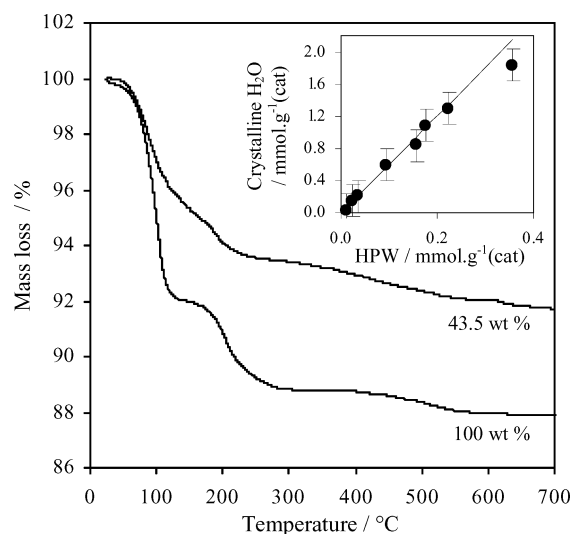


Fig. 2 Thermal analysis of HPW and HPW/ SiO_2 catalysts. Inset shows quantification of crystalline water from 200 °C weight loss.

Physisorbed water from both silica and heteropolyacid is lost at temperatures around 90–100 °C, and is present in all samples. In contrast the integral tertiary structural water in heteropolyacids is held more tightly and lost at around 200–220 °C. This second peak corresponds to a 3.3% weight loss in the bulk HPW sample which is equivalent to six water molecules, confirming the $\text{H}_3\text{PW}_{12}\text{O}_{40} \cdot 6\text{H}_2\text{O}$ stoichiometry. Further HPW decomposition commences at ~ 400 °C, with a slow, prolonged mass loss ($\sim 0.7\%$) corresponding to the reaction between acidic protons and structural oxygen from phosphotungstic acid releasing water, followed by decomposition to WO_3 and PO_x species.^{17,18}

A similar TGA profile was observed for all supported samples illustrated here for the 43.5 wt% sample, suggesting a common supported species. In bulk and high loaded samples loss of physisorbed and crystalline water occurs in distinct stages, with a trough between them in the DSC at ~ 155 °C. For low loading samples this distinction is less defined. However, assuming losses below 155 °C are dominated by desorption of physisorbed water, then a reasonable estimate of the crystalline water content lost between 155–220 °C can be obtained. In all catalysts above 3.6 wt% HPW this second mass loss correlated well with the existence of 6 crystalline water molecules from the adlayer (Fig. 2 inset).

Fig. 3 shows the DSC for the high temperature decomposition of the Keggin unit. The exotherm at ~ 620 °C represents complete decomposition of the Keggin structure to tungstate and phosphate species. The interaction between HPW and silica is evidenced by a slight fall in this decomposition temperature and thus slight destabilisation of the Keggin structure. The DSC peak area scales linearly with total HPW loading as expected, and as HPW content rises into the proposed multilayer regime (> 43.5 wt%), the exotherm moves towards that observed in the unsupported bulk heteropoly acid.

The nature of the adlayer and possible HPW crystallite formation was subsequently explored by XRD and EXAFS. Fig. 4 shows diffractograms for the supported HPW catalysts,

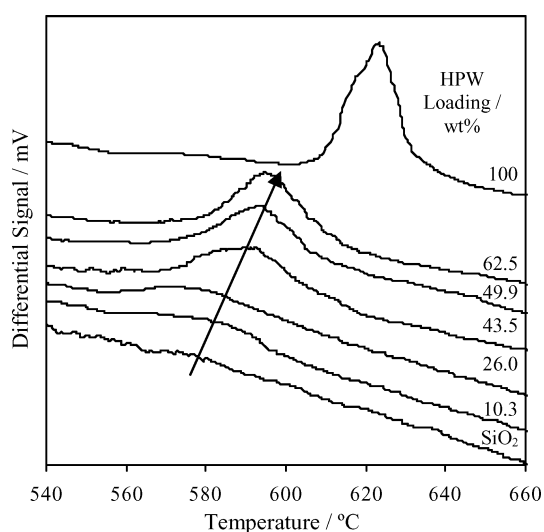


Fig. 3 DSC showing high temperature decomposition state for HPW and HPW/SiO₂ catalysts.

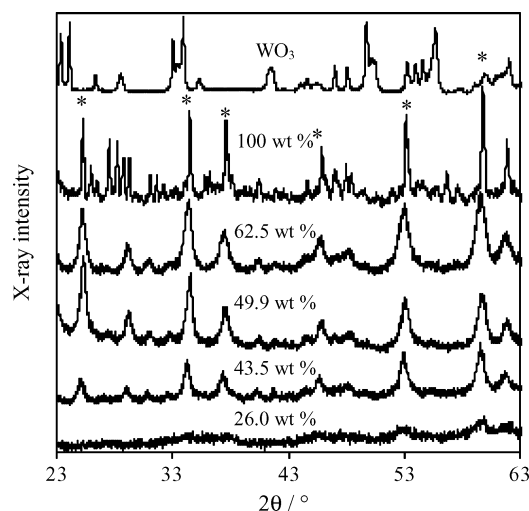


Fig. 4 Powder XRD of supported HPW/SiO₂ as a function of loading.

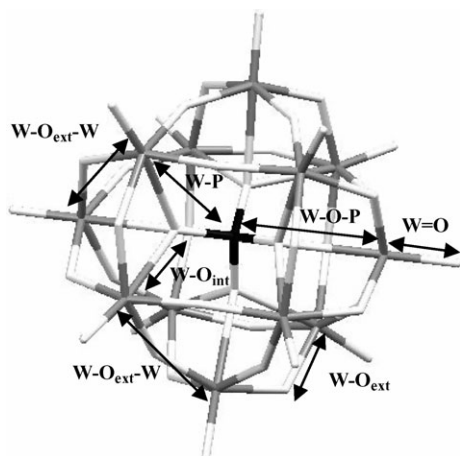
which reveal reflections characteristic of crystalline $\text{H}_3\text{PW}_{12}\text{O}_{40}$ (marked *). There were no reflections due to WO_3 suggesting negligible decomposition during preparation. Reflections for the supported HPW species also exhibit significant line broadening, indicating highly dispersed clusters. Volume-averaged particle sizes are given in Table 2, determined by application of the Scherrer equation¹⁹ to the 53.5 and 60° reflections, assuming cubeoctahedral aggregates. Even at loadings significantly above the proposed monolayer, the particle size of HPW clusters remains well below that observed in the unsupported material. Indeed cluster sizes for the multilayer regime do not vary significantly between 43.5 and 63 wt%, indicating HPW multilayers are also uniformly spread across the underlying SiO₂ interface.

Further insight into the local W chemical environment across the HPW/SiO₂ series was derived from XAS. Fig. 5a shows fitted W L_{III} EXAFS spectra for the 3.6 and 26 wt% HPW samples together with a calcined pure HPW sample. The structure of unsupported $\text{H}_3\text{W}_{12}\text{PO}_{40}$ clusters has been previously determined by EXAFS²⁰ and single crystal X-ray and neutron diffraction²¹ and is presented in Scheme 1, which highlights the different W environments. The fitted parameters for representative HPW/SiO₂ samples in Table 3 show excellent agreement with literature values for phosphotungstic acid, even at the lowest loading. This confirms the HPW Keggin units are adsorbed intact onto the silica support, consistent with our previous DRIFT and Raman measurements.¹⁶ Fig. 5b shows the corresponding radial distribution functions for these materials. It is interesting to note that the distribution

Table 2 Average particle size of supported HPW/SiO₂ catalysts^a

Catalyst	Particle size ± 1 nm
Pure unsupported HPW	48
Supported 43.5–63 wt%	12
Supported 26 wt%	6

^a Based on an average of the (532) and (732) reflections at 53.5 and 60°.



Scheme 1 Structure of the $\text{PW}_{12}\text{O}_{40}$ Keggin unit, with bond length assignments.^{22,23}

functions for the supported HPW samples are more consistent with those of pure HPW samples which have been calcined at 100°C to remove excess water of hydration. This suggests that the external $\text{W}=\text{O}$ and $\text{W}-\text{O}-\text{W}$ bonds may be perturbed by the presence of excess moisture.

XPS reveals that the surface tungstate environment is also perturbed at the silica interface. Fig. 6 inset shows a representative W 4f XP spectrum for the 43.5 wt% HPW sample, revealing a broad, poorly resolved doublet which can be deconvoluted into two distinct chemical states: a set of doublets at 35.3 eV ($4f_{7/2}$ component), consistent with that of the parent $\text{H}_3\text{PW}_{12}\text{O}_{40}$ heteropoly acid, together with a low bind-

ing set at 33.8 eV associated with a perturbed tungstate environment. The bulk-like HPW dominates the perturbed state by a constant $\sim 3 : 1$ ratio across the low loading (< 43.5 wt% W) range. Fig. 6 shows the loading dependencies of both surface tungstate species mirror each other during the low coverage regime, but their relative contributions rapidly diverge at higher loadings, indicative of a change in growth mode as may be expected upon multilayer/crystallite formation. The low BE tungstate state is rapidly attenuated at higher loadings, identifying its association with the interface.

There are two simple explanations for the origin of the perturbed W state prevalent at low coverages: either some of the HPW decomposes over the silica support yielding a mixed adlayer of intact Keggin units and a discrete WO_x phase; or the interface hosts intact Keggin units which contain electronically inequivalent W atoms. Our EXAFS measurements confirm the presence of intact Keggin units even at the lowest loadings which favour the latter hypothesis.

The acidic properties of the HPW/ SiO_2 series was subsequently investigated by a combination of pyridine titration to determine Brønsted *versus* Lewis character, and Hammett indicator measurements to assess the strength of the strongest acid sites. In addition, by taking advantage of size and polarity differences between the probe molecules, pyridine can provide useful insight into the total number of acid sites in supported heteropolyacids, whereas Hammett indicators focus on those acid sites accessible to large reactants. The Fig. 7 inset shows the DRIFTS spectra following pyridine adsorption. The parent SiO_2 sample exhibits two weak modes at 1442 and 1595 cm^{-1} which are characteristic of pyridine physisorbed or

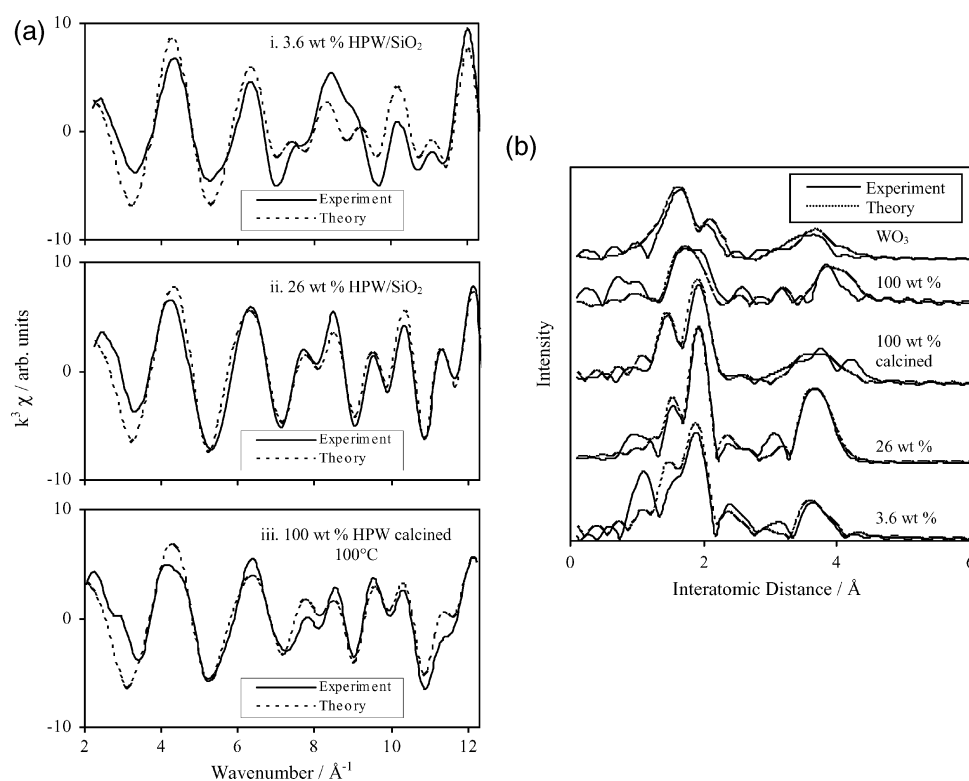


Fig. 5 (a) Fitted W L_{III} EXAFS of (i) 3.6 wt%; (ii) 26 wt% HPW/ SiO_2 and (iii) 100° calcined bulk HPW. (b) Fitted RDF of supported and bulk HPW samples and WO_3 .

Table 3 Structural parameters derived from fitted EXAFS for supported and bulk HPW samples

Sample	Parameter	Coordination environment					
		W=[O]	W-[O _{ext}]-W	W-[O _{int}]-W/P	W-O-[W]	W-O-[W]	W-O-[P]
3.6 wt% HPW/SiO ₂	N	1.4	4	1	2	2	
	R/Å	1.70	1.88	2.45	3.49	3.63	
	A	0.002	0.006	0.001	0.003	0.014	
26 wt% HPW/SiO ₂	N	1.2	4	1	2	2	1
	R/Å	1.72	1.91	2.45	3.45	3.73	3.55
	A	0.002	0.005	0.003	0.007	0.009	0.002
100 wt% HPW	N	1	4	1	2	2	1
	R/Å	1.47	1.83	2.35	3.54	3.74	3.48
	A	0.032	0.028	0.033	0.013	0.001	0.003
100 wt% HPW calcined	N	1.3	4	1	2	2	1
	R/Å	1.68	1.89	2.38	3.46	3.71	3.50
	A	0.001	0.008	0.017	0.014	0.009	0.002

bound to weak Lewis acid sites, most likely defective siloxane centres. New bands at 1484, 1531 1600 and 1630 cm⁻¹ appear upon impregnation with HPW, which are characteristic of Brønsted acid sites. These new bands grow with rising HPW loading.

The intensity of the 1531 cm⁻¹ band, attributed to Brønsted sites, increases linearly across the series while that due to physisorbed pyridine remains constant. Since pyridine is a small basic molecule, as well as binding to the catalyst surface it can also enter the pseudo-liquid bulk HPA phase. The observation that the number of acid sites scales directly with loading even for HPW multilayers demonstrates that all the supported Keggin units retain their acidity and are titratable.

The acid strength of the catalyst series was also explored by UV measurements on adsorbed Hammett indicators (Fig. 8). In contrast to pyridine, Hammett probes typically comprise bulky structures such as azo-linked phenyl derivatives, with consequently more limited access to bulk or interfacial sites. These measurements therefore reveal more about the catalytically significant, accessible surface acid sites. The very lowest loading catalysts ~3.6 wt% HPW were weakly acidic, with H_0

values between +2.8 and -3.0. The acid strength increases sharply during the preliminary stages of monolayer growth as HPW clusters spread across the support, with the Hammett acidity reaching a plateau between -11.3 > H_0 > -13.75 for samples with loadings above 10.3 wt% HPW/SiO₂.

A more detailed characterisation of the number and strength of acid sites was subsequently undertaken by NH₃ adsorption calorimetry. These measurements provide a detailed profile of the adsorption enthalpy (*i.e.* acid strength) as a function of NH₃ coverage (*i.e.* acid site density).²⁴ Fig. 9 shows the resulting calorimetry data from which it is immediately apparent that ΔH_{ads}^0 is independent of both HPW loading and NH₃ coverage for all samples ≥ 6.2 wt% HPW. This provides unequivocal evidence that a single type of strong acid site is present across the entire series, except during the very earliest stages of H₃PW₁₂O₄₀ deposition on silica. The NH₃ uptake, which is proportional to the number of acid sites, also scales with HPW loading. Table 4 summarises these results. An initial ΔH_{ads}^0 of -164 kJ mol⁻¹ is observed for all bar the lowest loading 3.6 wt% HPW/SiO₂ sample, for which a decrease to -138 kJ mol⁻¹ is observed. This is in line with our Hammett measurements, suggesting that the isolated

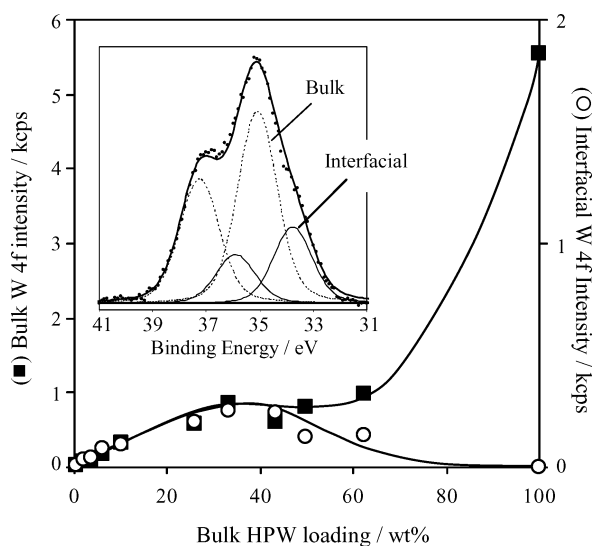


Fig. 6 XPS showing the variation of bulk and interfacial W species formed on HPW/SiO₂ as a function of HPW loading. Inset shows the deconvoluted W 4f spectrum from a 43.5 wt% HPW/SiO₂ sample.

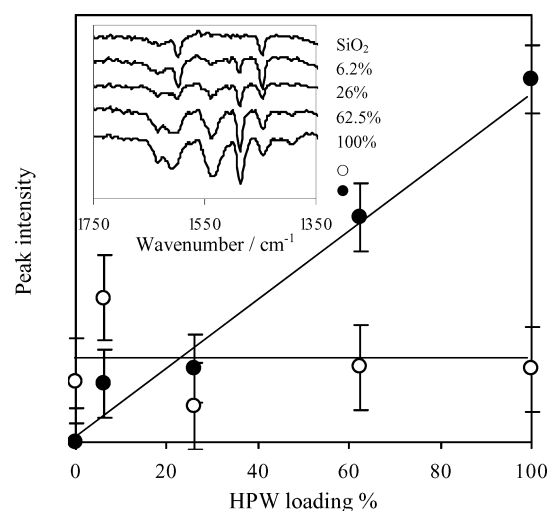


Fig. 7 Integrated intensity of Brønsted (●) 1531 cm⁻¹ and Lewis (○) 1442 cm⁻¹ pyridine IR bands. (Inset) DRIFT following pyridine titration of HPW/SiO₂ samples.

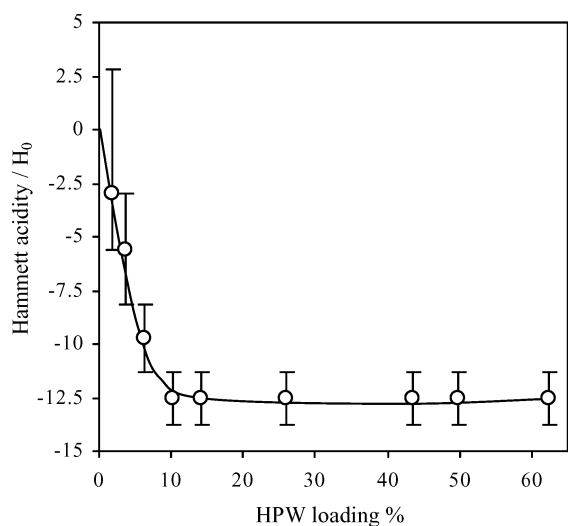


Fig. 8 Hammett indicator acid strength measurements of the series of HPW/SiO₂ catalysts.

Keggin units expected at such high dispersions exhibit weaker acidity, which may reflect the lack of crystalline water. The integrated NH₃ yields also approximate to three NH₃ molecules per Keggin for all but the 3.6 wt% sample, consistent with titration of all three protons initially present per Keggin in the parent heteropoly acid.

Catalyst activity

In order to understand the respective roles and catalytic applications of mono/multilayer adsorbed phosphotungstic acid, the HPW/SiO₂ series were screened for both liquid and gas phase, solid acid chemistries.

α -Pinene isomerisation

The catalytic performance of supported H₃PW₁₂O₄₀ towards the acid-catalysed isomerisation of α -pinene was explored. These transformations are sensitive to the strength of acid

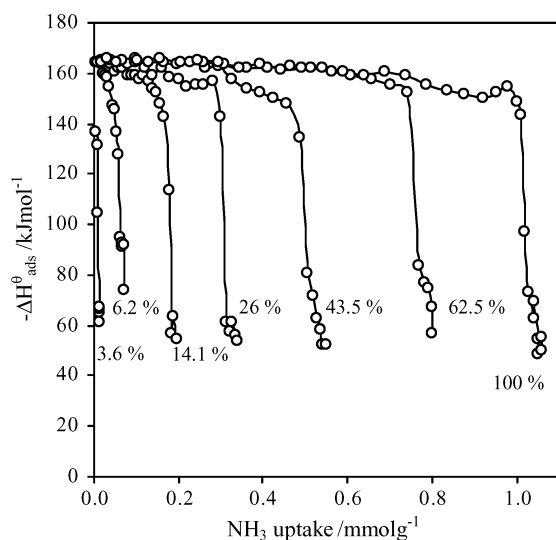


Fig. 9 NH₃ adsorption calorimetry data on the HPW and HPW/SiO₂ catalyst series.

Table 4 NH₃ calorimetry measurements on supported HPW samples^a

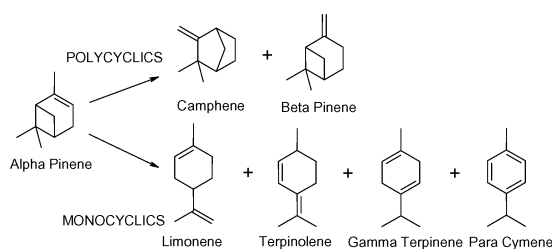
Sample	NH ₃ coverage/ mmol g ⁻¹ ^b	NH ₃ molecules per Keggin unit
Bulk HPW	1.02	2.95
62.5 wt%	0.74	3.42
43.5 wt%	0.48	3.21
26 wt%	0.299	3.31
14.1 wt%	0.177	3.6
6.2 wt%	0.063	2.92
3.6 wt%	0.0012	0.95

^a Samples degassed at 150 °C to avoid potential water displacement.
^b Defined as the NH₃ uptake when ΔH_{ads}^0 falls below 100 kJ mol⁻¹.

employed,^{25,26} with either ring opening to monocyclic products, or a rearrangement to bi- and possibly tri-cyclic products possible (Scheme 2), which renders the isomerisation a useful probe of solid acid strength. For example, increasing sulfur content within sulfated zirconias¹⁵ increases the limonene yield, indicating formation of the strong acid sites necessary for ring opening. Various pinene isomers have industrial and pharmaceutical value, hence controlling the selectivity of these transformations is also a commercially important issue to address.

Fig. 10a shows the α -pinene conversion across the series of catalysts after 100 min reaction at 30 °C. The catalysts were compared under low conversions to eliminate any artifacts due to mass transport limitations. Catalyst loadings below 3.6 wt% showed negligible reactivity towards α -pinene even after 24 h reaction, in line with their negligible acidity. The conversions exhibit a volcano-type reaction profile, with maximum conversion achieved for catalysts loaded between 26–43.5 wt% HPW. It is important to note the poor performance of the pure parent acid. In contrast α -pinene conversion shows a strong linear correlation with the concentration of our designated interfacial tungstate species (as determined by XPS), shown in the inset of Fig. 10a. The initial turnover frequency was determined for the 26 wt% HPW catalyst to be 68.5 mmol h⁻¹ g(cat)⁻¹.

Since both α -pinene and its isomers are relatively large, non-polar molecules, their diffusion into the secondary structure formed by aggregation of Keggin units within HPW multilayers (analogous to the pseudo-liquid phase in bulk HPW), is unlikely. Accessible acid sites are therefore expected to be localised at external Keggin surfaces, with no catalytic contribution from bulk HPW material. The maximum surface area/number of exposed Keggin clusters should therefore be achieved around the saturation HPW monolayer point



Scheme 2 Isomerisation of α -pinene.

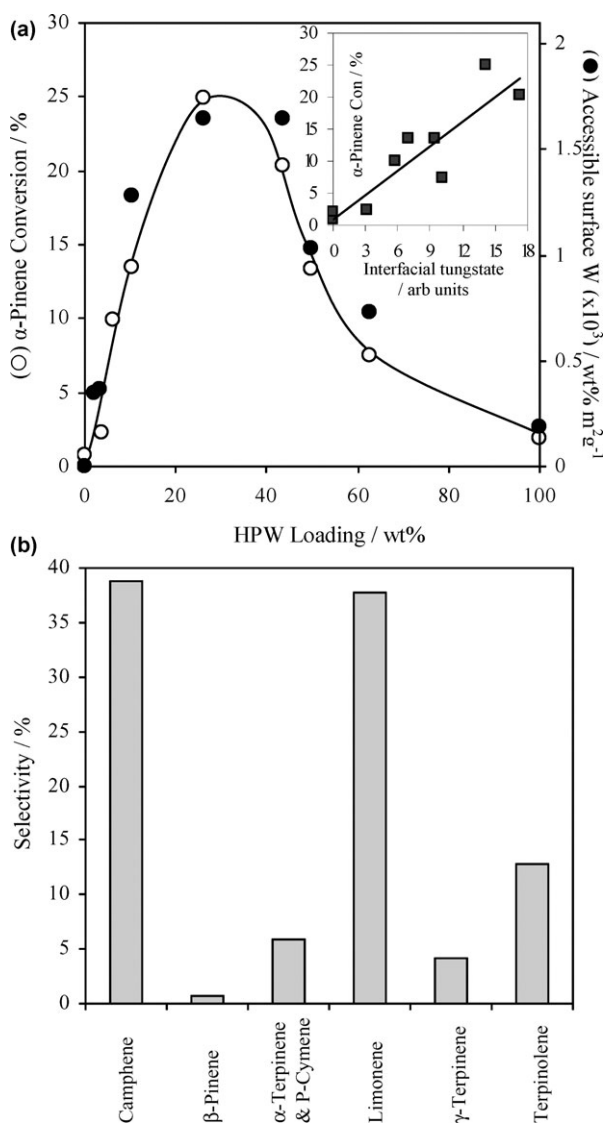


Fig. 10 (a) Correlation between conversion of α -pinene after 100 min reaction at 30 °C and accessible surface W as a function of HPW loading. Inset shows correlation of α -pinene conversion with interfacial tungstate intensity from XPS. (b) Product selectivity observed after 100 min reaction of α -pinene over a 26 wt% HPW/SiO₂ catalyst at 30 °C.

(~40 wt%), precisely where the pinene conversion peaks in Fig. 10a. Beyond 43.5 wt% HPW α -pinene conversion drops off due to pore blockage effects as 3D clusters and multilayers of the Keggin unit builds up.

The major products for all catalysts were camphene and limonene in accordance with the literature.¹⁵ Camphene and β -pinene were the only polycyclic products detected at significant levels, whereas a number of monocyclic products were seen (see Scheme 2). Other than limonene, terpinolene is the major product formed with ~13% selectivity. Terpinolene is closely related to limonene, with both formed *via* deprotonation of the p-menthenyl cation formed by ring opening of pinene.¹⁴

Fig. 10b shows the typical product distribution obtained during α -pinene isomerisation. Monocyclic (major product

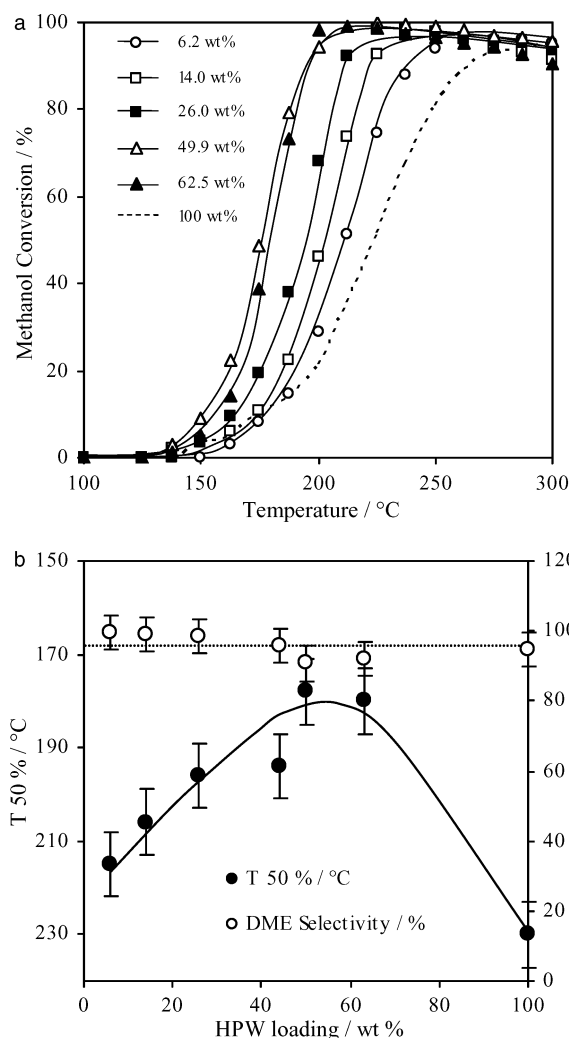


Fig. 11 Light off curves for methanol conversion over HPW/SiO₂ catalysts. (b) $T_{50\%}$ and steady state DME selectivity at 300 °C following methanol condensation over HPW/SiO₂ catalysts.

limonene) and polycyclic (major product camphene) products were generated in approximately equal amounts irrespective of catalyst loading. Limonene formation confirms that strong acid sites are present across the HPW/SiO₂ series. The independence of selectivity on HPW loading correlates well with the NH₃ calorimetry results which predict a common acid site strength ≥ 6.2 wt%. In summary, the conversion scaled with the number of interfacial tungstate sites up to the monolayer, but the acidity of active sites was constant across the series, unlike sulfated zirconias, wherein sulfur loading strongly influences both acid site density and strength.¹⁵

Methanol condensation

The performance of the supported HPW materials was also screened in methanol condensation to dimethylether (DME) and water. This is a relatively simple bimolecular reaction involving small polar reactants and products, and therefore has the potential to capitalise upon additional acid sites present within the extended HPW structures formed at higher loadings.

As observed during α -pinene isomerisation, the lowest loaded catalysts (<6.2 wt%) proved largely ineffective with no methanol condensation observed. This again correlates with acidity measurements which revealed that loadings below 6.2 wt% only possess weak acid sites and suggests that while structurally the Keggin unit is intact, their acidity is decreased by site isolation. Fig. 11a and b show that as the HPW loading is increased the light off temperature steadily decreases, reaching a limiting value of ~ 169 °C for the highest loading catalysts. All supported catalysts ≥ 6.2 wt% HPW exhibited greater activity and lower $T_{50\%}$ for methanol conversion than the unsupported HPW sample. These results correlate well with (steady state) isothermal GC results which were used to calculate reaction selectivity. At maximum conversion levels above 175 °C activity reached 33 mmol L cat⁻¹ s⁻¹ over the 0.25 ml catalyst bed. All active catalysts exhibited >99% selectivity towards DME when reactions were performed <250 °C. At higher temperatures an increase in methanol to gasoline (MTG) type chemistry²⁷ was observed at the expense of DME formation, with hydrocarbon products ethane and/or ethene resulting from breakdown of MeOH and/or DME observed.

In contrast to α -pinene isomerisation, MeOH conversion did not pass through a maximum between 26 and 43.5 wt%, instead it reached a plateau at high loadings. This may reflect differences in the polarities of these processes: methanol condensation involves polar reactants and products and can thus occur in the pseudo-liquid bulk in addition to surface acid sites. Methanol conversion therefore scales with total HPA content, whereas α -pinene isomerisation scales with the completion of the monolayer dispersed HPW, which itself passes through a maximum at 26–43.5 wt%.

There have been previous reports of reduced acid strength in low loaded HPW/SiO₂ samples which were ascribed to strong interaction with the support.²⁸ Clearly this study demonstrates that loss of acid strength for HPW loadings <6.2 wt% is not due to decomposition of the Keggin structure, rather that the high dispersion results in an inability to form crystalline H₂O between adjacent Keggin units. Given that we estimate the monolayer saturation occurs at ~ 44 wt% HPW, we thus propose that there is a threshold HPW coverage of

~ 0.14 ML at which point it is possible to form tetramers with a pocket for crystalline water as illustrated in Scheme 3.

Conclusions

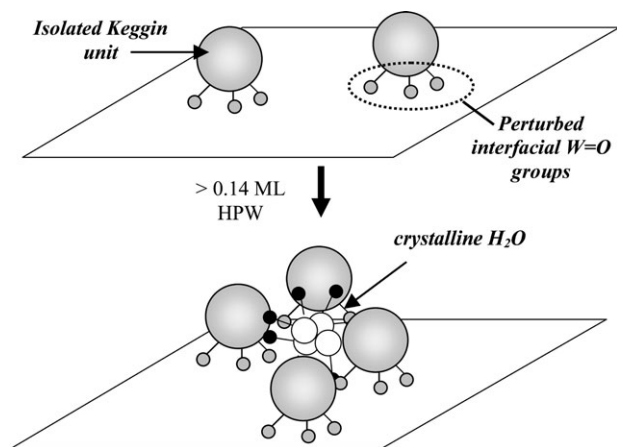
A series of SiO₂ supported H₃PW₁₂O₄₀ catalysts have been prepared and fully characterised. Structurally we find that the Keggin unit remains intact on immobilisation and the acid site strength is identical for all loadings >6.2 wt%. During the evolution of the monolayer inequivalent W environments can be observed by XPS which are in a 3 : 1 ratio. These are attributed to perturbation of Keggin W atoms which are in direct contact with the SiO₂ surface. NH₃ calorimetry measurements reveal that the acid strength is invariant of loading ≥ 6.2 wt% HPW and is comparable to the strength of bulk HPW species. Structural characterisation using EXAFS confirms that the Keggin unit is intact for all loadings, suggesting the decrease in acid strength <6.2 wt% HPW is attributable to the presence of highly dispersed clusters which are unable to form crystalline water between adjacent Keggin units. We propose that there is a threshold HPW coverage of ~ 0.14 ML at which point it is possible to form tetramers with a pocket for crystalline water. The observed trends in catalyst activity are consistent with the acid strength measurements. For reactions involving non-polar hydrocarbon substrates optimum catalyst activity is observed when the interfacial species and thus accessible tungstate species is maximised. In contrast the activity of supported HPW catalysts in polar reactions, which can take advantage of the pseudo-liquid phase, scales with loading.

Acknowledgements

Financial support by the UK Engineering and Physical Sciences Research Council under grants GR/M20877/01 and GR/R39436/01, and from BP Chemicals is gratefully acknowledged.

References

- 1 R. A. Sheldon, *Chem. Ind.*, 1997, **1**, 12.
- 2 I. V. Kozhevnikov, *Cat. Rev. Sci. Eng.*, 1995, **37**, 311.
- 3 M. T. Pope, *Heteropoly and Isopoly Oxometalates*, Springer-Verlag, Berlin, 1983.
- 4 I. V. Kozhevnikov, *Chem. Rev.*, 1998, **98**, 171.
- 5 K. Nowińska, R. Fórmaniak, W. Kaleta and A. Wąclaw, *Appl. Catal., A*, 2003, **256**, 115.
- 6 K. Pamin, A. Kubacka, Z. Olejniczak, J. Haber and B. Sulikowski, *Appl. Catal., A*, 2000, **194–195**, 137.
- 7 E. López-Salinas, J. G. Hernández-Cortéz, I. Schifter, E. Torres-García, J. Navarrete, A. Gutiérrez-Carrillo, T. López, P. P. Lottici and D. Bersani, *Appl. Catal., A*, 2000, **193**, 215.
- 8 Y. Izumi and K. Urabe, *Chem. Lett.*, 1981, 663.
- 9 T. Blasco, A. Corma, A. Martínez and P. Martínez-Escolano, *J. Catal.*, 1998, **177**, 306.
- 10 F. Lefebvre, *J. Chem. Soc., Chem. Commun.*, 1992, 756.
- 11 V. M. Mastikhin, S. M. Kulikov, A. V. Nosov, I. V. Kozhevnikov, I. L. Mudrakovsky and M. N. Timofeeva, *J. Mol. Catal.*, 1990, **60**, 65.
- 12 M. S. Kaba, I. K. Song, D. C. Duncan, C. L. Hill and M. A. Barteau, *Inorg. Chem.*, 1998, **37**, 398.
- 13 L. P. Hammett and A. J. Deyrup, *J. Am. Chem. Soc.*, 1932, **54**, 2721.



Scheme 3 Evolution of dispersed HPW clusters on SiO₂ support.

- 14 G. Gündüz, R. Dimitrova, S. Yilmaz, L. Dimitrov and M. Spassova, *J. Mol. Catal. A: Chem.*, 2004, **225**, 253.
- 15 M. A. Ecomier, K. Wilson and A. F. Lee, *J. Catal.*, 2003, **215**, 57.
- 16 A. D. Newman, A. F. Lee and K. Wilson, *Catal. Lett.*, 2005, **102**, 45.
- 17 B. W. L. Southward, J. S. Vaughan and C. T. O'Connor, *J. Catal.*, 1995, **153**, 293.
- 18 B. K. Hodnett and J. B. Moffat, *J. Catal.*, 1984, **88**, 253.
- 19 P. Scherrer, *Nachr. Ges. Wiss. Goettingen, Math. Phys. Kl.*, 1918, **2**, 98.
- 20 J. Evans, M. Pillinger and J. M. Rummey, *J. Chem. Soc., Dalton Trans.*, 1996, **14**, 2951.
- 21 G. M. Brown, M. R. Noe-Spirlet, W. R. Busing and H. A. Levy, *Acta Crystallogr., Sect. B*, 1977, **33**, 1038.
- 22 A. Kremenovic, A. Spasojevic-de Bire, R. Dimitrijevic, P. Sciau, U. B. Mioc and P. Columban, *Solid State Ionics*, 2000, **132**, 39.
- 23 J. F. Keggin, *Proc. R. Soc. London, Ser. A*, 1934, **144**, 75.
- 24 S. P. Felix, C. Savill-Jowitt and D. R. Brown, *Thermochim. Acta*, 2005, **33**, 59.
- 25 Stanislaus and L. M. Yeddanapalli, *Can. J. Chem.*, 1972, **50**, 61.
- 26 M. K. Yadav, C. D. Chudasama and R. V. Jasra, *J. Mol. Catal. A: Chem.*, 2004, **216**, 51.
- 27 M. Stöcker, *Microporous Mesoporous Mater.*, 1999, **29**, 3.
- 28 E. F. Kozhevnikova and I. V. Kozhevnikov, *J. Catal.*, 2004, **224**, 164.